A periplasmic metallochaperone (PmcY) couples Zn^{2+}-transport to sensing in *Pseudomonas aeruginosa*

Running title: An anchored membrane protein couples YiiP mediated Zn^{2+} efflux to Zn^{2+} sensing in *Pseudomonas aeruginosa*

Paula Mihelj[1], Tomás Moreyra[1], Monserrat Olea-Flores[2], María Elena Carrizo[3], Teresita Padilla-Benavides[2], Daniel Raimunda[1]

[1]Instituto de Investigaciones Médicas Mercedes y Martín Ferreyra, INIMEC.

[2]Department of Molecular Biology and Biochemistry, Wesleyan University, Middletown CT, 06459, USA.

[3]Centro de Investigaciones en Química Biológica de Córdoba CIQUIBIC.

[1, 3] CONICET-Universidad Nacional de Córdoba. Argentina.

Abstract

Pseudomonas aeruginosa thrive to survive in harsh conditions imposed by the host. We have previously described two Zn^{2+}-transporting members of the Cation Diffusion Facilitator family, YiiP and CzcD, inhibiting susceptibility to imipenem by decreasing the expression of the outer membrane porin OprD (A. Salusso and D. Raimunda, Frontiers in cellular and infection microbiology 7:84, 2017, https://doi.org/10.3389/fcimb.2017.00084). Here we provide evidence that a protein encoded in *yiiP´*s operon, PA3962, is fundamental to the coupling of these processes. Immunodetection assay indicates that PA3962 locates in membranes. Supporting a role in *oprD* regulation, a PA3962 insertional mutant has a significant increase of *oprD* expression levels and imipenem sensitivity, which is suppressed by gene complementation but not in presence of Zn^{2+}, as opposed to the YiiP mutant. We identified 2 pairs of conserved acidic residues in a hydrophobic juxtamembrane domain. Metal binding specificity and stoichiometry was explored in wild-type and mutant versions of these. Zn^{2+} appears as the cognate metal of PA3962, with residues D40, D47 and D65 required for its coordination. As the periplasmic Zn^{2+}-sensor CzcS regulates *oprD* expression, the interaction with it was analyzed *in vitro*. Interaction was Zn^{2+}-dependent, and mutations of D47A or D65A abolished it. We propose a role for PA3962, hereafter periplasmic metallochaperone of YiiP (PmcY), in the context of Zn^{2+} signaling pathways in *P. aeruginosa*. The relay YiiP–PmcY, supplies Zn^{2+} and activates CzcS/CzcR, down-regulating the transcription of the imipenem-permeable OprD. This mechanism would allow *P. aeruginosa* to put a

brake on unspecific mechanisms for micronutrient uptake, with potential xenobiotic entry, while the cytosolic Zn^{2+} quota is still sufficient.

Introduction

Pseudomonas aeruginosa is a facultative anaerobic gram-negative bacteria and a prevalent opportunistic pathogen in respiratory infections of patients diagnosed with cystic fibrosis (1). It is considered an oligotrophic organism with a highly dynamic capacity for antibiotic resistance, metabolic adaptation, or phenotypical switching, which sometimes translates to fitness costs (2). Metabolic adaptations and antibiotic resistance involve optimization of Zn^{2+} usage in niches with low bioavailability (3). In the first case, the Zn^{2+}-dependent (C+) to Zn^{2+}-independent (C-) isoform switching of ribosomal subunits, increases the intracellular Zn^{2+} pool in this condition (4). In the second, Zn^{2+} induces carbapenem resistance by repressing the transcription, and then the antibiotic influx, of the outer membrane porin Occ1, also known as OprD (5). As carbapenem-resistant OprD mutants show enhanced fitness *in vivo* (6) we hypothesize that this “master of survival”, could benefit from a last resort-type of intracellular Zn^{2+} availability by finely tuning Zn^{2+}-sensing mechanisms. In this way this opportunistic pathogen could adapt metabolically and become resistant to carbapenems, avoiding the pay-offs of a fitness cost imposed by nutritional immunity(7).

We have previously shown that the Zn^{2+} exporters of the Cation Diffusion Facilitator family, YiiP and CzcD regulate levels of OprD (8). Single insertion mutants of these genes showed increased sensitivity to imipenem, and increased Zn^{2+} sensitivity

when introduced into double mutant backgrounds where other Zn^{2+} resistance mechanisms were also affected. Considering studies by others showing that transcription of *czcD* responds to Zn^{2+} levels in the growth media with a slow temporal activation (9) a role in Zn^{2+} detoxification might be considered. However, the fact that *yiiP* transcripts are not upregulated by Zn^{2+}, opens new possibilities for the role of this Zn^{2+}-transporter in Zn^{2+} mediated signaling.

Zn^{2+} sensing mechanisms in *P. aeruginosa* are well known. At the cytoplasmic level, CadR, a member of the MerR transcription factor family, controls the expression of CadA, also known as ZntA, a Zn^{2+}-transporting P_{IB}-ATPase (8, 10). Interestingly, it has been proposed that under high Zn^{2+} conditions, CadA is required for timely expression of CzcCBA, also known as HME-RND, a tripartite Zn^{2+}-export system that promotes efflux from the periplasm to the extracellular space (10). This implies that the specific CadA Zn^{2+}-export is coupled to Zn^{2+} sensing in the periplasm. In line with this, extracellular Zn^{2+} bioavailability in *P. aeruginosa* is primarily detected in the periplasm via the two-component system (TCS) CzcS-CzcR. CzcS senses periplasmic Zn^{2+} by coordinating the metal in the periplasmic domain (11), which is transduced to cytosolic domains promoting autophosphorylation of the histidine kinase domain and finally, the transphosphorylation to CzcR. Phosphorylated CzcR (P-CzcR) has dual effects on transcription of genes in the CzcS-CzcR regulon (12). For example, P-CzcR up-regulates transcription of HME-RND, thus counteracting a potential Zn^{2+} overload (9, 10) in the periplasm. However, P-CzcR affects negatively the transcription of genes involved in pyocyanin synthesis and of the outer membrane porin *oprD* (11, 12).

Here we present evidence suggesting that a periplasmic metallochaperone of YiiP (PmcY/PA3962) is required for *oprD* repression and thus, for Zn^{2+} sensing in the periplasm. Our data shows that PmcY is a Zn^{2+}-metallochaperone that interacts with CzcS, its putative acceptor or target protein. We also propose that the intracellular Zn^{2+} efflux to the periplasm mediated by YiiP-PmcY has coevolved in Pseudomonadales as a mechanism for limiting the fitness cost of adapting to common environmental or host-imposed scenarios with low Zn^{2+} bioavailability, by repressing an unspecific outer membrane porin.

Materials and methods

Bacterial strains, plasmids and growth media conditions

Pseudomonas aeruginosa MPAO1 wild-type (WT), and the insertion mutants *yiiP::dTn5* and *pmcY*/PA3962*::dTn5* were obtained from the *P. aeruginosa* Mutant Library at the University of Washington ((13); Table 1). For complementation of the *pmcY*/PA3962*::dTn5* strain PA3962 locus plus the 250bp upstream bases was PCR amplified and cloned in pSEVA621 using EcoRI and KpnI sites (14). The sequence for *gfp* was introduced at the 3'-end as a fusion in order to promote protein stability using KpnI and XbaI sites. Electrocompetent cells were transformed by electroporation as described (15) and selected on Luria–Bertani (LB) agar plates supplemented with gentamicin (30 µg/ml). Double mutant *oprD-pmcY* (DM3004) was obtained via double recombination events following methods previously described (16). The up and down-stream 500 bp fragments of PA3962 were amplified and stiched by PCR. After purification and digestions with EcoRI and

HindIII restriction enzymes the fragment was ligated into the suicide plasmid pEX18-Gm. Electrocompetents *oprD::dTn5* cells were transformed with this plasmid and recombinants were selected on LB-agar supplemented with 60 µg/ml gentamicin. Several colonies were grown in LB supplemented with sucrose 5%. The PA3962 locus deletion was confirmed by PCR using genomic DNA of isolated colonies grown in LB + sucrose 5%, supplemented with tetracycline (30 µg/ml). The primers used in these and other procedures are listed in Table 1.

Plasmid constructions and protein expression and purification

In a first attempt to yield a whole version of PmcY by heterologous expression in *E. coli* PA3962 locus was cloned from *P. aeruginosa* MPAO1 gDNA and inserted by ligation in the expression plasmids pET23b(+) (Novagen) or pGEX4T-2 using primers described in Table 1. These constructs contained at C-terminal a hexahistidine ($(His)_6$) tag preceded by Tobacco Etch Virus (TEV) protease recognition site. Due to low yield of the protein and guided by bioinformatics analyses we expressed the juxtamembrane domain of PmcY ($PmcY_j$) as a GST fusion protein by deletion of N- and C-termini and $(His)_6$ tag of PmcY by the one-step site-directed deletion PCR protocol (17). Site directed mutagenesis of conserved residues were obtained using the same procedure. Similarly, the soluble domain (SD) of CzcS (amino acids 40-166, $CzcS_{SD}$) was cloned by PCR amplification from MPAO1 gDNA and ligated in pET16bStrep (Table 1) with a twin-strep tag at N-terminal. All constructs and mutants were confirmed by DNA sequencing.

For protein expression and purification *E. coli* BL21(DE3)pLysS were transformed with one of the above constructs. After selection cells were grown in LB overnight at

37°C on a shaker at 200 rpm. Next day 1-2 L of LB media with antibiotic was inoculated with cells to reach OD_{600}= 0.1 and grown in the same conditions till early log-phase. At this point cultures were induced with 0.15 mM IPTG for 16 h at 20°C. For purification of GST and GST fusion versions of $PmcY_j$ cells were resuspendend in 50 ml of Tris-HCl 20 mM pH 7.5, NaCl 500 mM, TCEP 0.25 mM, 0.1% Triton X-100 (Buffer A) plus PMSF 1 mM, and lysed in a cell disruptor EmulsiFlex C3 (Avestin). After ultracentrifugation at 100,000 *g* the supernatant was incubated with 1 ml of Glutathione Sepharose 4B or Fast Flow (GE Healthcare) for 1 h at room temperature. Resin was packed by gravity in a polypropylene column (Bio-Rad) and washed with 30 resin volumes of buffer A. The fusion protein was eluted with buffer A containing 40 mM glutathione. The soluble domain for CzcS was expressed and purified as described earlier (11) with minor modifications. After growth and induction cells were lysed as above and ultracentrifuged at 100,000 *g*. The supernatant was incubated for 1 h at room temperature with 0.5 ml of Strep-Tactin resin (IBA Lifesciences) equilibrated with buffer A for 1 h and eluted after washing with 30 resin volumes. Bound protein was eluted with 10 resin volumes of buffer A containing 50 mM of D-biotin. In both cases elution fractions were analyzed by SDS-PAGE 12%, Coomassie brilliant blue staining and Western blot using $(His)_6$-tag antibody (pAb, Rabbit, Genscript), GST-tag antibody (pAb, Rabbit, Genscript) or StrepMAB-Classic antibody (IBA Lifesciences) as primary antibodies. Those fractions containing protein were pooled for dialysis in buffer A using a dialysis tubing (SnakeSkin, Thermo Scientific) with 3.5 kDa cut-off. After addition of 10% glycerol, protein concentration was estimated by Bradford (Bio-Rad) and 280 nm lectures in NanoDrop (Thermo Scientific). Protein samples were frozen and maintained at -

80°C for later use. For in-column interaction assays the bait protein, GST-PmcY$_j$ WT and mutant versions, were not eluted from the resin and kept at 4°C in the dark for later use and store for no more than 2 weeks. In this case protein concentrations were determined by densitometry. Denatured resin samples were run in SDS-PAGE 12%, stained with Coomassie brilliant blue (CBB) and images analyzed with ImageJ (18). For calibration, bovine serum albumin (Sigma-Aldrich) standards were run in the same gel.

Antibiotic sensitivity assays

Susceptibility to imipenem (Sigma-Aldrich) and ciprofloxacin was assessed by the agar dilution or the inhibition halo methods in Müller–Hinton (MH) medium as described before (8). For agar dilution overnight grown cells were serially diluted from an initial OD_{600}= 1 and then 10 µl were spotted on MH agar plates with different antibiotic concentrations. For inhibition halos, a suspension of cells at OD_{600}=0.05 in soft agar were layered on top of MH agar plates. After solidifying, 7-mm diameter filter paper discs embedded with the indicated amount of imipenem were located on top of the soft agar. In all cases growth or inhibition was evaluated after overnight incubation at 37°C. Analyses of the imipenem MIC values found by agar dilution method (ADM) *vs*. our previously data published using Epsilon-test method (Biomerieux Diagnostics) yielded a lineal correlation between MICs following $y=8.082\ x$ with and $R^2 = 0.797$, where y equals the apparent ADMs MICs, and x the Epsilon-test ones. Thus, apparent imipenem concentrations are informed in this work.

Quantitative RT-PCR analysis

Overnight cultures from *P. aeruginosa* WT, *yiiP::dTn5* and *pmcY::dTn5* were diluted to an OD_{600} of 0.05 in LB and incubated until they reached an OD_{600} of 0.6-0.8. Total RNA was extracted with TRIzol™ Reagent (Invitrogen) according to the supplier's instructions and treated with RNase-free DNase I (TransGen Biotech) for 2 h at 37°C to remove residual DNA. After phenol/chloroform extraction, RNAs were precipitated with ethanol and the pellets resuspended in RNase-free water. For cDNA synthesis, 200-300 ng of RNA was reverse transcribed using random primers and *EasyScript*® Reverse Transcriptase (TransGen Biotech) according to the manufacturer's instructions. Quantitative PCR was performed using FastStart Universal SYBR Green Mastermix (Rox) (Roche), according to the supplier's instructions. Fold change expression levels were calculated using the $2^{-\Delta\Delta Ct}$ method as previously described (19). Results were normalized with the *rpsL* gene (PA4268). Primers used for qPCR studies are listed in Table 1.

Metal binding assays

Transition metal (TM) binding capacity of GST fusion proteins was evaluated using the chromogenic dye 4-(2-Pyridylazo) resorcinol (PAR, Tokyo Chemical Industry). For incubation of the proteins with TM we followed described protocols for in-solution (20) or in-column (21) assays with some modifications. To assess binding to proteins 10-20 µM samples (or the mass bound to resin to yield this concentration before adding PAR) were incubated for 30 min with 5 molar excess of TM in buffer A. For in-solution binding assays unbound TM were separated by exclusion chromatography with Sephadex G25-80 (Sigma-Aldrich) and for the in-column type

the resin was washed with 10 volumes of buffer A to remove unbound TM. Before TM quantification protein concentrations were estimated as described earlier and samples containing proteins in solution or bound to resin were treated with 0.4-0.8 mg/ml of proteinase K. For TM quantification, PAR was added to a final concentration of 100 µM and read in microplates at 500 nm. Calibration curves were done in parallel for each TM and the molar ratio of protein to TM calculated. In both conformations GST alone or GST fusions were run in parallel to detect TM bound in proteins as purified. These values represented no more than 10% of those found in TM incubated samples and were subtracted in all cases. For the quantification of Mn^{2+} the buffer pH was modified from 7.5 to 11 as the colorimetric reaction of this TM is more sensitive. Therefore, after the digestion reaction with proteinase K, the samples were evaporated completely and resuspended in 200 mM CAPS (3-(Cyclohexylamino)-1-propanesulfonic acid) buffer pH 11.

Protein localization

The *E. coli* strain BL21(DE3)pLysS transformed with the plasmid pET-23b(+)-PA3962, which expresses the PA3962 protein fused to a 6-histidine tag, was grown in 12.5 ml of LB medium at 37°C for 16 h. This culture was placed in two flasks with 500 ml of LB medium and grown with shaking (200 rpm) at 37°C for 1 h. One of the cultures was induced with 0.15 mM of IPTG and the other was used as a control (basal). After 3 h of growth the cells were harvested by centrifugation at 4,000 *g*, 4°C for 10 min. Cell pellets were washed in ice-cold 30 ml of 50 mM Tris-HCl pH 7.5 and 0.3 M sorbitol (buffer S) 3 times, with addition of 10 µM EDTA in the second wash. Cells were pelleted by centrifugation at 9,000 *g*, 4°C for 10 min. Finally, cells were

resuspended in 30 ml of ultrapure water and incubated for 5 min at room temperature. They were then centrifuged at 11,000 *g*, 4°C for 30 min. The supernatants were collected and centrifuged again to eliminate any possible contamination. After this they were considered the periplasmic fractions. For cytosolic and total membrane fractions cell pellets were resuspended in 7 ml of 10 mM Tris-HCl pH 7.5 and disrupted at 4°C using a tip sonicator (Vibra Cell, Sonics & Materials, Inc.) with 6 cycles of 20 seconds on and 60 seconds off pulses. The lysate was centrifuged at 6,000 *g* for 10 min at 4°C to remove undisrupted cells and centrifuged again at 100,000 *g* for 30 min at 4°C. The supernatants were recovered and classified as cytoplasmic fractions. The resultant pellets were resuspended in 5 ml of 10 mM Tris-HCl pH 7.5 and classified as total membrane fractions. The protein concentration of all fractions was quantified by Bradford assay, and those with a value less than 1 mg/ml were concentrated using centrifuge filtration tubes (Centricon, Millipore). Samples of all fractions were prepared at concentrations of 1 mg/ml and 5X Laemmli sample buffer was added. A final total protein mass of 10 µg was loaded per lane on 14% SDS-PAGE gels in duplicate, one for CBB staining and the other for Western blot. $(His)_6$-tag antibody (pAb, Rabbit, Genscript) and anti-rabbit antibody labeled with horseradish peroxidase were used to detect expression in fractions. Images were taken using Amersham Image Quant 800 Fluor (Cytiva).

Protein-protein interaction assay

To evaluate the interaction between PmcY and CzcS, the recombinant proteins GST-$PmcY_j$ (WT and mutants D40A, D47A, and D65A) and $CzcS_{SD}$ were used. A 100±20 mg sample of purified WT or mutant versions of GST-$PmcY_j$ were treated

with EDTA-Tris. For this, Glutathione Fast Flow (GE Healthcare) resin with bound protein was incubated with 1 ml of buffer A plus 1 mM EDTA-Tris in a 10 ml polypropylene chromatography column (Bio-Rad). Three ml of buffer A were used to remove residual EDTA from column. The interaction was tested in two conditions, with GST-PmcY$_j$ loaded with (+Zn^{2+}) and without (-Zn^{2+}) $ZnCl_2$. For this, resin was incubated for 5 min with 500 µl of 100 µM $ZnCl_2$ in buffer A or just buffer A, respectively. The CzcS$_{SD}$ protein was used in solution and previously treated with 0.5 mM EDTA-Tris for 30 min in ice. EDTA-Tris was removed with PD-10 column equilibrated in buffer A. In-column GST-PmcY$_j$ and mutant versions, in its two conditions (+Zn^{2+}) and (-Zn^{2+}), were incubated with 25 µM CzcS$_{SD}$, added in 250 µl, during two passes through the column (Flow through, FT) and 4 washes (W1-4) were performed with 250 µl of buffer A. Finally, the resin was resuspended in 250 µl of buffer A and samples prepared with 5X Laemmli loading buffer for SDS-PAGE 12% analyses. After CBB staining images were taken using Amersham Image Quant 800 Fluor (Cytiva).

Bioinformatics analyses

To analyze the conservation of residues in a putative PmcY family, homologs were searched in a local database of all protein sequences of RefSeq reference and representative genomes protein sequences (Refseq_select_prot) (January 2024) by the reciprocal best hit (RBH) method (19). Four hundred and sevenunique organisms having PmcY-like members with unique accession numbers were found. Multiple sequence alignment (MSA) was done in Clustal Omega (22) using a similar number

of sequences and the same MSA was used in ChimeraX (23) to create the amino acids conservation map in the putative 3D AF structure of PA3962 (AF-Q9HX54-F1). This number of organisms were used later to compare and create a list of non-redundant bacterial organisms having, or not, the *pmcY-yiiP* architecture. The search of the *pmcY-yiiP* operon was done using Multigenblast (24). Similar RBH searches were performed for OprD and CzcS homologs in the same data base. After removal of duplicated organism names, a 4-group diagram was prepared with these organisms (https://bioinformatics.psb.ugent.be/webtools/Venn/) and a phylogenetic tree was constructed for visualization of coevolution in iTOL (25).

Results

PA3962 is a membrane protein

PA3962 is part of a putative operon with YiiP (PA3963). Previous bioinformatics studies of identified *P. aeruginosa* secreted proteins pointed that the N-terminal sequence in PA3962 is a type II signal peptide (26). These results were supported with a plasmid library screening in *E. coli* where several PAO1 genomic DNA fragments, including PA3962, fused to truncated alkaline phosphatase (PhoA) drove its periplasmic localization. Signal peptides are recognized by different secretion systems in bacteria and classified in different groups. The type II are related to proteins anchored to the membrane, also called lipoproteins. A consensus sequence called “lipobox” is found in the type II signal peptide, which allows for molecular recognition by the machinery involved in processing and finally anchoring the protein to the inner or outer membrane. For this, first a conserved cysteine residue in the

lipobox is diacylated with diacylgycerol. Second, the signal peptide is removed by a specific protease leaving free and reactive the amino group of the cysteine for a final third acylation (27). Figure 1, shows the predicted structure of PA3962 by AlphaFold2 (AF2) (28) showcasing the colour–coded hydrophobic profile generated in ChimeraX and position of Cys23 in the lipobox. The ribbon structures depict the putative position of the protein facing the periplasmic space after the anchoring occurs. In order to confirm the membrane localization of PA3962 we expressed the whole protein with a C-terminal $(His)_6$ tag in *E. coli* in basal and induced conditions. After fractioning cells, cytosolic, total membranes, and periplasmic samples were analyzed by SDS-PAGE and Western blot using anti-$(His)_6$ as primary antibody (Fig. 1B). Protein detection was evident in most of the fractions and signal was increased under basal conditions, pointing to an inhibitory effect of the translation in presence of the inducer when the full length protein is overexpressed. Most importantly the detection in total membrane fraction was observed. As the mass of protein loaded in all lanes was similar, and assuming an equal contribution of each compartment in cell mass, a qualitative conclusion is that PA3962 is a membrane protein. PhoA detection in *E. coli* requires folding in the periplasm, thus this orientation is the most likely scenario in *P. aeruginosa* and we renamed PA3962 as Periplasmic metallochaperone of YiiP, PmcY.

PmcY is involved in *oprD* mediated imipenem susceptibility

As previous results indicated a role for YiiP in Zn^{2+}-dependent antibiotic susceptibility involving OprD and altered membrane permeability (8) we next analyzed if absence of PmcY yielded similar effects. The minimal inhibitory concentration (MIC) for the

antibiotic in Tn5-generated mutant strains (Fig. 1C) YiiP and PmcY mutants showed that both are sensitive to imipenem *vs.* WT. Complementation of PmcY strain was achieved by transformation of mutant cells with the low copy plasmid pSEVA621 (14) carrying PA3962 locus under transcriptional regulation of 250 bp upstream sequence (Fig. 1D). We have previously demonstrated that lack of YiiP induces expression of OprD (8). If PmcY is involved in imipenem susceptibility the expression of *oprD* should be altered compared to the WT strain. The results of *oprD* locus expression between PmcY and YiiP mutant strains (*vs*. WT) correlates to the imipenem susceptible phenotype of both (Fig 1E). These results indicated that the molecular mechanism leading to the loss of imipenem susceptibility involves the lack of Zn^{2+} sensing capacity. This loss would involve specifically Zn^{2+} transport from cytosol to the periplasm. Thus, we hypothesized that both, YiiP and PmcY, mutants would remain sensitive to imipenem at high Zn^{2+} content (0.5 mM) in the growth media. However, only PmcY mutant strain showed the same imipenem susceptibility in presence of high levels of Zn^{2+} indicating a key role for PmcY. The apparent dispense of YiiP to sense Zn^{2+} at high extracellular Zn^{2+} conditions, correlates with a save-for-later strategy to sustain steady-state levels of the intracellular quota of this vital element. To test the Zn^{2+}-specificity of the mechanism we tested also ciprofloxacin sensitivity (Fig. 1F right). The lack of Zn^{2+} complementation to this antibiotic susceptibility observed in both mutants, points to the involvement of another mechanism likely related to membrane permeability of ciprofloxacin and other more lipophilic antibiotics, as suggested previously (8). To discard any agonistic effects between OprD and PmcY related to membrane permeability, we generated the double mutant *oprD-pmcY* (DM3004) and evaluated its imipenem

susceptibility. Figure 1G shows that both strains, *oprD::Tn5* and DM3004, behave similarly. These results indicate that PmcY is required for Zn^{2+} sensing in the periplasm and that *oprD* is regulated by PmcY activity. Thus we focused on the pivotal role of PmcY as part of a sensing mechanism leading to decrease intrinsic imipenem susceptibility, and hypothesize that PmcY should bind Zn^{2+} and interact with a sensor to likely transfer the metal to it.

PmcY binds Zn^{2+} specifically through conserved aspartate residues

We hypothesized that PmcY plays a role as metallochaperone. These function in metalation of proteins or in detoxification pathways, and in both cases the commonality is their capacity to bind a specific transition metal through conserved residues. A multiple sequence alignment of PmcY homologs obtained by a reciprocal best hit search in complete bacterial genomes allowed us to identified conserved residues (Fig. 2A, maroon). Most of these would be located in a periplasmic domain juxtaposed to the membrane. Conserved amino acids are all acidic, with oxygen (O) ligands of lateral chains of aspartates and glutamates. After several failed trials of full length PmcY expression and purification to get enough protein for biochemical characterization, we opted to fuse this domain (amino acids 30 to 93), which we called PmcY juxtamembrane ($PmcY_j$), to GST. The fusion protein was purified and its capacity and specificity to bind transition metals analyzed. For this, five molar excess of different metals were incubated with the fusion protein (Fig. 2B-C) and after unbound metal was separated by exclusion chromatography (Fig. 2B) or washed (Fig. 2C), protein was quantified and metal bound to protein detected as described. This strategy allowed us to confirm that Zn^{2+} is the cognate metal for

PmcY and that the stoichiometry of binding is 2 Zn^{2+} per PmcY molecule. To identify possible binding sites, we analyzed the Zn^{2+} binding of the single mutants of highly conserved positions with O ligands; *i.e.*, D40A, D47A and D65A. All these mutations lowered the binding stoichiometry to 1, indicating their likely participation in two Zn^{2+} binding sites. A closer look to the distances between O atoms in lateral chains of the PmcY structure, underscores residues D47-D65 as candidates for one Zn^{2+} binding with the archetypical tetrahedral geometry (Fig. 2D).

PmcY interacts with the periplasmic Zn^{2+} sensor CzcS

Another property which defines a metallochaperone is the interaction with its target(s) protein(s). This is key in order to promote the ligand transfer reaction, and the metal transfer, between the donor, the metallochaperone, and the acceptor, the target protein. Thus an interaction between PmcY and CzcS could promote Zn^{2+} sensing by means of a ligand transfer reaction between partners. In order to test this, we expressed and purified the periplasmic soluble domain (SD) of CzcS (amino acids 40 to 166, named $CzcS_{SD}$) as described by Wang et al. (11) with a twin Strep-tag at the N-terminal end. The protein preparation was treated with EDTA to eliminate Zn^{2+} carried-over during purification, and then incubated with GST-PmcYj, in two conditions, EDTA-treated or loaded with Zn^{2+}. After collecting flow through and washes we detected the presence of CzcS in the final resin (Rf) only when GST-$PmcY_j$ was loaded with Zn^{2+} (Fig. 3A, black asterisk). In order to assess how Zn^{2+} occupancy affected this interaction, GST-$PmcY_j$ mutants, D40A, D47A and D65A were analyzed similarly. The Zn^{2+}-dependent interaction was lost only in D47A and D65A mutants. This data supports the hypothesis in which these acidic residues

might coordinate Zn^{2+} in one binding site. Mutation D40A did not preclude the interaction in presence of Zn^{2+}.

PmcY-YiiP operon coevolved with OprD and CzcS in Pseuodomonadales

The data presented suggest that YiiP, PmcY, CzcS/CzcR participate in a sensing mechanism coupling Zn^{2+} efflux via YiiP, to decrease imipenem suceptibility (as *oprD* expression is downregulated). If this mechanism is conserved among gram-negative bacteria, we hypothesized that PmcY homologs found in other organisms would present the same operon architecture as in *P. aeruginosa* MPAO1. A multigene BLAST search did not support this. However, organisms presenting the operon architecture were mostly of the Pseudomonadales order. Most importantly, contrasted with organisms with non-*pmcY-yiiP* operon detected, *oprD* and *czcS* were mostly distributed in organisms with the operon *pmcY-yiiP*; *i.e.*, the Pseudomonadales order. The lack of CzcS in a high number of members in this clade is surprising. However, the periplasmic Cu^{+} sensor CopS has also been proposed to downregulate *oprD* transcription (29). Altogether these data support a likely coevolution of these genes. We discuss in the next section what could be the selection pressure of the coevolution and the physiological role in a context of Zn^{2+} bioavailability.

Discussion

The association between the Zn^{2+} induced repression of *oprD* transcription, and the Zn^{2+} induced resistance to imipenem is long recognized (30). Moreover, several studies have used this response to dissect important molecular and mechanistic

aspects of the CzcS-CzcR signaling pathway (11, 31) in the periplasmic space. Here we present evidence pointing to the participation of YiiP and PmcY in periplasmic Zn^{2+}-sensing mechanisms. In particular, we propose that both players affect *oprD* transcription, and likely other genes, by promoting Zn^{2+}-sensing; *i.e.*, the metalation of the Zn^{2+} sensor CzcS. We provide evidences supporting our model, showing that PmcY binds Zn^{2+}, with high specificity and with a molar stoichiometry of 2 Zn^{2+} per molecule. Metal coordination is given by mean of conserved Asp residues. Phenotypical analyses showed that different to WT and YiiP mutant, the mutant strain of PmcY lacks the Zn^{2+}-dependent response to imipenem susceptibility likely by a lack or reduced Zn^{2+}-sensing capacity of CzcS. These results lead us to propose PmcY as a Zn^{2+}-metalochaperone.

Many of the players involved in orchestrating Zn^{2+} homeostasis in *P. aeruginosa* have been described (32). High Zn^{2+} bioavailability is sensed by periplasmic and cytosolic sensors, CzcS and CadR, respectively which lead to transcription of high capacity Zn^{2+} transport systems, such as HME-RND and P_{IB}-type ATPases (9, 10). The integration of these compartmentalized sensing mechanisms can be interpreted considering electrochemical Zn^{2+} gradient. As Zn^{2+} entries and accumulates first in the periplasm transcription of HME-RND are first expected. However, free Zn^{2+} is almost negligible in cells (33) and a role for cytosolic Zn^{2+} exporters have been proposed in periplasmic Zn^{2+} sensing mechanisms (10). This is important as it suggests the participation of Zn^{2+}-transport systems allowing cross-talk between cellular compartments to promote intracellular Zn^{2+} exit even when extracellular Zn^{2+} could turn into lower levels.

Could a similar scenario, involving Zn^{2+} transport systems, participate in cross-talk between compartments when Zn^{2+} bioavailability is low? Considering the risk of losing Zn^{2+} in such scenario, the process should be accompanied of a “favourable” fitness cost. We proposed that Zn^{2+}-export by YiiP is linked to Zn^{2+}-sensing by CzcS with the final outcome of delaying *oprD* expression, which role allows entry of nutrients, but also xenobiotic molecules such as antibiotics. Thus this hypersensitivity to sense intracellular Zn^{2+}, when scarce but still available, would be beneficial for this opportunistic pathogen as *oprD* induction is still repressed.

HME-RND also is part of the CzcS-CzcR regulon (31) and Zn^{2+}-binding to CzcS upregulates the transcripts levels. Even when transcription could be triggered by YiiP-PmcY activity we speculate that low Zn^{2+} availability is not sufficient to promote HME-RND activity as this transport system would have similar biochemical properties to CadA; i.e.: high transport capacity but low metal affinity. Incidental Zn^{2+}-entry via OprD has been suggested (34). Although counterintuitive, the up-regulation of HME-RND by CzcS activation, would prepare the cell for a potential Zn^{2+} overflow in the periplasm with minimal basal activity of HME-RND until Zn^{2+} bioavailability increases. However, evidence to support this is still missing and the lack of Zn^{2+} resistance shown by OprD mutants contradicts this role (31).

Lastly, and considering our working model, although it is tempting to hypothesize that a Zn^{2+}-basic amino acid abduct could be the physiological substrate transported by OprD, the metal-chelating molecule EDTA was not able to outcompete arginine/lysine transport by OprD in *in vitro* studies (5). Nonetheless, considering the Zn^{2+} binding capacity of several xenobiotics, including antibiotics, and the evident

lack of specificity of *oprD* for carboxylated substrates, its overexpression could be viewed as a “razors-edge”-like situation promoting Zn^{2+} uptake linked to the xenobiotc molecule carrying the ion. Thus, braking the system could be beneficial until Zn^{2+} reservoirs are downsized to the limits of a “go-hunting” for survival condition.

Conflict of interest statement

All authors declare that research was conducted in the absence of any commercial or financial relationships.

Author contributions

Conceived and designed the experiments: D.R., P.M.

Analyzed the data: D.R., P.M., T.M., M.E.C.

Contributed reagents/samples/analysis/tools: D.R., M.E.C., M.O.-F., T.P.-B.

Wrote or edited the manuscript: D.R., P.M.

All authors read and approved the final manuscript.

Funding

This work was supported by the Agencia Nacional de Promoción Científica y Tecnológica (ANPCyT) PICT-2018-03139 to D.R., and PICT-2021-0147 to M.E.C. D.R. and M.E.C. are Consejo Nacional de Investigaciones Científicas y Tecnológicas (CONICET) investigators. P.M. is recipient of a CONICET doctoral

fellowship. T.M. is recipient of a doctoral fellowship from ANPCyT (PICT-2018-03139). T.P.-B. was supported by Wesleyan University institutional funds.

Abbreviations

TM, transition metal; CDF, cation diffusion facilitator; IPTG, Isopropyl β-D-1-thiogalactopyranoside; PAR, 4-(2-Pyridylazo) resorcinol; HME-RND, heavy metal exporter of the resistance-nodulation-division family.

Acknowledgments

We thank Camila Semeniuk, Dr. Laura Montroull and Dr. Andrea Pellegrini for their invaluable help during this work.

References

1. Rossi E, La Rosa R, Bartell JA, Marvig RL, Haagensen JAJ, Sommer LM, Molin S, Johansen HK. 2021. Pseudomonas aeruginosa adaptation and evolution in patients with cystic fibrosis. Nature Reviews Microbiology 19:331-342.
2. Zhu M, Dai X. 2024. Shaping of microbial phenotypes by trade-offs. Nat Commun 15:4238.
3. Panina EM, Mironov AA, Gelfand MS. 2003. Comparative genomics of bacterial zinc regulons: enhanced ion transport, pathogenesis, and rearrangement of ribosomal proteins. Proc Natl Acad Sci U S A 100:9912-7.
4. Pederick VG, Eijkelkamp BA, Begg SL, Ween MP, McAllister LJ, Paton JC, McDevitt CA. 2015. ZnuA and zinc homeostasis in Pseudomonas aeruginosa. Sci Rep 5:13139.
5. Eren E, Vijayaraghavan J, Liu J, Cheneke BR, Touw DS, Lepore BW, Indic M, Movileanu L, van den Berg B. 2012. Substrate specificity within a family of outer membrane carboxylate channels. PLoS Biol 10:e1001242.
6. Skurnik D, Roux D, Cattoir V, Danilchanka O, Lu X, Yoder-Himes DR, Han K, Guillard T, Jiang D, Gaultier C, Guerin F, Aschard H, Leclercq R, Mekalanos JJ, Lory S, Pier GB. 2013. Enhanced in vivo fitness of carbapenem-resistant oprD mutants of Pseudomonas aeruginosa revealed through high-throughput sequencing. Proc Natl Acad Sci U S A 110:20747-52.
7. Kehl-Fie TE, Skaar EP. 2010. Nutritional immunity beyond iron: a role for manganese and zinc. Curr Opin Chem Biol 14:218-24.

504 8. Salusso A, Raimunda D. 2017. Defining the Roles of the Cation Diffusion Facilitators in
505 Fe(2+)/Zn(2+) Homeostasis and Establishment of Their Participation in Virulence in
506 Pseudomonas aeruginosa. Front Cell Infect Microbiol 7:84.
507 9. Ducret V, Abdou M, Goncalves Milho C, Leoni S, Martin-Pelaud O, Sandoz A, Segovia Campos
508 I, Tercier-Waeber ML, Valentini M, Perron K. 2021. Global Analysis of the Zinc Homeostasis
509 Network in Pseudomonas aeruginosa and Its Gene Expression Dynamics. Front Microbiol
510 12:739988.
511 10. Ducret V, Gonzalez MR, Leoni S, Valentini M, Perron K. 2020. The CzcCBA Efflux System
512 Requires the CadA P-Type ATPase for Timely Expression Upon Zinc Excess in Pseudomonas
513 aeruginosa. Front Microbiol 11:911.
514 11. Wang D, Chen W, Huang S, He Y, Liu X, Hu Q, Wei T, Sang H, Gan J, Chen H. 2017. Structural
515 basis of Zn(II) induced metal detoxification and antibiotic resistance by histidine kinase CzcS
516 in Pseudomonas aeruginosa. PLoS Pathog 13:e1006533.
517 12. Dieppois G, Ducret V, Caille O, Perron K. 2012. The transcriptional regulator CzcR modulates
518 antibiotic resistance and quorum sensing in Pseudomonas aeruginosa. PLoS One 7:e38148.
519 13. Held K, Ramage E, Jacobs M, Gallagher L, Manoil C. 2012. Sequence-verified two-allele
520 transposon mutant library for Pseudomonas aeruginosa PAO1. J Bacteriol 194:6387-9.
521 14. Martinez-Garcia E, Fraile S, Algar E, Aparicio T, Velazquez E, Calles B, Tas H, Blazquez B,
522 Martin B, Prieto C, Sanchez-Sampedro L, Norholm MHH, Volke DC, Wirth NT, Dvorak P,
523 Alejaldre L, Grozinger L, Crowther M, Goni-Moreno A, Nikel PI, Nogales J, de Lorenzo V.
524 2023. SEVA 4.0: an update of the Standard European Vector Architecture database for
525 advanced analysis and programming of bacterial phenotypes. Nucleic Acids Res 51:D1558-
526 D1567.
527 15. Choi KH, Schweizer HP. 2006. mini-Tn7 insertion in bacteria with single attTn7 sites: example
528 Pseudomonas aeruginosa. Nat Protoc 1:153-61.
529 16. Huang W, Wilks A. 2017. A rapid seamless method for gene knockout in Pseudomonas
530 aeruginosa. BMC Microbiol 17:199.
531 17. Liu H, Naismith JH. 2008. An efficient one-step site-directed deletion, insertion, single and
532 multiple-site plasmid mutagenesis protocol. BMC Biotechnol 8:91.
533 18. Schneider CA, Rasband WS, Eliceiri KW. 2012. NIH Image to ImageJ: 25 years of image
534 analysis. Nature Methods 9:671-675.
535 19. Mihelj P, Abreu I, Moreyra T, Gonzalez-Guerrero M, Raimunda D. 2023. Functional
536 Characterization of the Co(2+) Transporter AitP in Sinorhizobium meliloti: A New Player in
537 Fe(2+) Homeostasis. Appl Environ Microbiol 89:e0190122.
538 20. Raimunda D, Subramanian P, Stemmler T, Arguello JM. 2012. A tetrahedral coordination of
539 Zinc during transmembrane transport by P-type Zn(2+)-ATPases. Biochim Biophys Acta
540 1818:1374-7.
541 21. Modrof J, Becker S, Muhlberger E. 2003. Ebola virus transcription activator VP30 is a zinc-
542 binding protein. J Virol 77:3334-8.
543 22. Madeira F, Madhusoodanan N, Lee J, Eusebi A, Niewielska A, Tivey ARN, Lopez R, Butcher S.
544 2024. The EMBL-EBI Job Dispatcher sequence analysis tools framework in 2024. Nucleic
545 acids research 52:W521-W525.
546 23. Meng EC, Goddard TD, Pettersen EF, Couch GS, Pearson ZJ, Morris JH, Ferrin TE. 2023. UCSF
547 ChimeraX: Tools for structure building and analysis. Protein Sci 32:e4792.
548 24. Medema MH, Takano E, Breitling R. 2013. Detecting sequence homology at the gene cluster
549 level with MultiGeneBlast. Mol Biol Evol 30:1218-23.
550 25. Letunic I, Bork P. 2024. Interactive Tree of Life (iTOL) v6: recent updates to the phylogenetic
551 tree display and annotation tool. Nucleic Acids Res 52:W78-W82.

552 26. Lewenza S, Gardy JL, Brinkman FS, Hancock RE. 2005. Genome-wide identification of
553 Pseudomonas aeruginosa exported proteins using a consensus computational strategy
554 combined with a laboratory-based PhoA fusion screen. Genome Res 15:321-9.
555 27. El Rayes J, Rodriguez-Alonso R, Collet JF. 2021. Lipoproteins in Gram-negative bacteria: new
556 insights into their biogenesis, subcellular targeting and functional roles. Curr Opin Microbiol
557 61:25-34.
558 28. Jumper J, Evans R, Pritzel A, Green T, Figurnov M, Ronneberger O, Tunyasuvunakool K, Bates
559 R, Zidek A, Potapenko A, Bridgland A, Meyer C, Kohl SAA, Ballard AJ, Cowie A, Romera-
560 Paredes B, Nikolov S, Jain R, Adler J, Back T, Petersen S, Reiman D, Clancy E, Zielinski M,
561 Steinegger M, Pacholska M, Berghammer T, Bodenstein S, Silver D, Vinyals O, Senior AW,
562 Kavukcuoglu K, Kohli P, Hassabis D. 2021. Highly accurate protein structure prediction with
563 AlphaFold. Nature 596:583-589.
564 29. Caille O, Rossier C, Perron K. 2007. A copper-activated two-component system interacts
565 with zinc and imipenem resistance in Pseudomonas aeruginosa. J Bacteriol 189:4561-8.
566 30. Conejo MC, Garcia I, Martinez-Martinez L, Picabea L, Pascual A. 2003. Zinc eluted from
567 siliconized latex urinary catheters decreases OprD expression, causing carbapenem
568 resistance in Pseudomonas aeruginosa. Antimicrob Agents Chemother 47:2313-5.
569 31. Perron K, Caille O, Rossier C, Van Delden C, Dumas JL, Kohler T. 2004. CzcR-CzcS, a two-
570 component system involved in heavy metal and carbapenem resistance in Pseudomonas
571 aeruginosa. J Biol Chem 279:8761-8.
572 32. Ducret V, Gonzalez D, Perron K. 2023. Zinc homeostasis in Pseudomonas. Biometals 36:729-
573 744.
574 33. Maret W. 2013. Zinc biochemistry: from a single zinc enzyme to a key element of life. Adv
575 Nutr 4:82-91.
576 34. Wang S, Cheng J, Niu Y, Li P, Zhang X, Lin J. 2021. Strategies for Zinc Uptake in Pseudomonas
577 aeruginosa at the Host-Pathogen Interface. Front Microbiol 12:741873.

Tables

578 **Table 1.** List of Strains, plasmids and primers used in this study.

Strain/plasmid/primer	Relevant characteristics/sequence	Reference/Use
Pseudomonas aeruginosa		
MPAO1	Wild-type	Held *et al.* (2012)
yiiP::dTn5	Tn5 derivative ISphoA/hah insertion in *yiiP* (PA3963), Tc^r	Held *et al.* (2012)
pmcY::dTn5	Tn5 derivative ISphoA/hah insertion in *pmcY* (PA3962), Tc^r	Held *et al.* (2012)
C-pmcY	Tn5 derivative ISphoA/hah insertion in *pmcY*, pSEVA621-P_{pmcY}-*pmcY-gfp, Tc^r Gm^r*	This work
oprD::dTn5	Tn5 derivative ISphoA/hah insertion in *pmcY* (PA0958), Tc^r	Held *et al.* (2012)
DM3004	Tn5 derivative ISphoA/hah insertion in *pmcY* (PA0958), ΔPA3962,Tc^r	This work
Escherichia coli		
BL21(DE3) pLysS	*F- ompT hsdSB* (rB-mB-) *gal dcm* (DE3) *pLysS* (Cam^r)	Invitrogen, Carlsbad, CA,USA
DH5α	*supE44* Δ*lacU169* (φ80 *lacZ* ΔM15*) hsdR17 recA1 endA1 gyrA96 thi1 relA1*	Invitrogen, Carlsbad, CA,USA
Plasmids		
pET23b(+)	T7 expression plasmid, Ap^r	Novagen, Darmstadt, Germany
pGEX-4-T2	T7*lac* expression plasmid*,* Ap^r	Cytiva, Marlborough, MA, USA
pSEVA621	RK2 cloning plasmid, Gm^r	Martínez-García *et al.* 2023
pET16bStrep	T7 expression plasmid, Ap^r	Luis Rubio´s laboratory
pEX18-Gm	*oriT*$^+$ *sacB*$^+$, gene replacement vector with MCS from pUC18, Gm^r	Huang & Wilks (2017)
Primers		

F- pET PA3962	CAGTCATATGCGCCTTGCCACCCGCG	Cloning PA3962 in pET23b(+) + NdeI at 5'-end
R- pET PA3962	ACTCGAGGGACTGAAAATACAGGTTTTCGCCGCCG CCGCGCTTCAGGCC	Cloning PA3962 in pET23b(+) + TEV site + XhoI at 3'- end
F-pGEX PA3962	GGATCCATGCGCCTTGCCACCCGCG	Cloning PA3962 in pGEX4T-2 + BamHI at 5'-end
R-pGEX PA3962	CCCGGGTCAGTGGTGGTGGTGGTGGTGCTCGAGG GACTGAAAATACAGGTTTTCGCCGGCGGCCGGCTT CAGGCC	Cloning in pGEX4T-2 + TEV site + $(His)_6$ tag + SmaI at 3'-end
F-pGEX-$_{1-29}$PA3962	CGTGGATCCGAGCGACGCGGCCAGATCGACGGTC G	Deletion N-terminal residues (1-29) of PmcY
R-pGEX-$_{1-29}$PA3962	TCGCTCGGATCCACGCGGAACCAGATCCGATTTTG	Deletion N-terminal residues (1-29) of PmcY
F-pGEX-$_{94-138}$PA3962	GCGGACGGCGGCGAAAACCTGTATTTTCAGTCCCT	Deletion C-terminal residues (94-138) of PmcY
R-pGEX-$_{94-138}$PA3962	TTCGCCGCCGTCCGCGCCGACGGCATCCTTGAGCA	Deletion C-terminal residues (94-138) of PmcY
F-pGEX$_{30-93}$PA3962His*6	CGGACGGCTGATCTAGACTAGGGGTCGACTCGAGC GGC	Deletion of $(His)_6$ tag
R-pGEX$_{30-93}$PA3962His*6	TCTAGATCAGCCGTCCGCGCCGACGGCATCCTTGA GCAC	Deletion of $(His)_6$ tag
F-D40xA– PA3962	TCGCATCGCCCCGGCCATCGTCGCCTTCGACGCCA TCGGCC	D40A mutation in $PmcY_j$
R-D40xA– PA3962	GCCGGGGCGATGCGACCGTCGATCTGGCCGCGTC GCTC	D40A mutation in $PmcY_j$
F-D47xA– PA3962	CGCCTTCGCCGCCATCGGCCTGCTGTTCTATATCAT CCCCGGCCTG	D47A mutation in $PmcY_j$

R-D47xA– PA3962	GATGGCGGCGAAGGCGACGATGGCCGGATCGATGCGACCG	D47A mutation in $PmcY_j$
F-D65xA– PA3962	CGGCGTCGCCTTCGCCACCGGCGCCATCTACCTGCCCGAC	D65A mutation in $PmcY_j$
R-D65xA– PA3962	GCGAAGGCGACGCCGAAGGCGATCAGGCCGGGGATGATATAGAACAGC	D65A mutation in $PmcY_j$
F-pSEVA PA3962	CTAGTGAATTCCCCGGGTGGTCTTGCCGGC	Cloning *pmcY* plus 250pb up stream + EcoRI at 5'-end
R-pSEVA PA3962	ACTGGTACCGGCGGCCGGCTTCA	Cloning *pmcY* plus 250pb up stream + KpnI at 3'-end
F-GFP	AGGGTACCGCTAGCAAAGGAGAA	Cloning *gfp* + KpnI at 5'-end
R-GFP	CCTTCTAGATTAGCAGCCGGATCCT	Cloning *gfp* + XbaI at 3'-end
F-CzcS	ATCCATATGGCCCGCGAGCGGGA	Cloning *czcS* soluble domain + NdeI at 5'-end
R-CzcS	AGTGGATCCTCATTTTCGAACTGCGGGTGGCTCCAGCGCTCGTCGGCGT	Cloning *czcS* soluble domain plus StrepII + BamHI at 3'-end
F-RpsL	TCGGCACTGCGTAAGGTATG	qRT-PCR
R-RpsL	CTTACGGTCTTTGACACCCG	qRT-PCR
F-OprD	GCACAAACGATGAAGGCAAG	qRT-PCR
R-OprD	GTAGGCCAAGGTGAAAGTGT	qRT-PCR
F-up500bp	ACGTAAGCTTAGGCCGACACCGTCCAGCGC	*pmcY* deletion in *P. aeruginosa*
R-up500bp	GGTCGCGCTCGGAGGGCGGAGTATGACCTCCGGGTGAACATGACG	*pmcY* deletion in *P. aeruginosa*
F-down500bp	CGTCATGTTCACCCGGAGGTCATACTCCGCCCTCCGAGCGCGACC	*pmcY* deletion in *P. aeruginosa*

R-down500bp	ACGTGAATTCTCTGGAAGGCCAGGAGAAGG	*pmcY* deletion in *P. aeruginosa*

Figure legends

Figure 1. PmcY is a membrane protein that counteracts imipenem susceptibility. (A) Left, hydrophobic surface profile of the AF2 predicted structure for PmcY/PA3962. Position of Cys23 is indicated. Center and right, ribbon diagram of PmcY with lipobox amino acids indicated in green. The thiol group of Cys23 would promote acylation anchoring the protein, right. Notice that independent of the position at the inner or the outer membrane, PmcY faces the periplasmic space. P= periplasm; M= membrane; I/O= inside/outside the cell. (B) Analysis of heterologously expressed PmcY-$(His)_6$ in *E. coli* compartments (cytosolic= C; total membranes= TM; periplasm= P) by cell fractioning. Ten µg of protein from each fraction obtained from cells grown in LB media (basal= B; induced = I) were analyzed by SDS-PAGE (left) and Western blot (right). PmcY-$(His)_6$ expression is apparently increased in basal conditions and mostly found in the membrane fraction. (C) Serial dilutions (10 µl) of *P. aeruginosa* PAO1 (WT), *pmcY::dTn5* and *yiiP::dTn5* cells initially at OD_{600nm}=1.0 were spotted on MH-agar supplemented with the indicated imipenem concentration and incubated for 16 h at 37°C. (D) Complementation of *pmcY::dTn5* restores imipenem susceptibility. PA3962 plus 250bp upstream bases were cloned in the low copy plasmid pSEVA621 as a fusion to GFP. This construct was introduced by electroporation into *pmcY::dTn5*. No complementation was observed in *pmcY::dTn5* cells transformed with empty pSEVA621 nor with pSEVA621-GFP (not shown) (E) Fold change expression levels ($2^{-\Delta\Delta Ct}$ with *rpsL* as reference gene) of *oprD* transcripts *vs.* WT. Cells were grown until mid-log phase at 37°C in LB before RNA extraction. Data are the mean ± SE of three independent experiments. *,

P<0.05 from a two-tailed Student's t test of averaged ΔCt (*vs.* WT). (F) Zn^{2+} induced lack of susceptibility response is specific to imipenem and is PmcY dependent. Notice that *pmcY::dTn5* is unresponsive to Zn^{2+} and the lack of response to ciprofloxacin in presence of the TM in both mutant strains. Agar dilution method was used to determine MICs. (G) Double mutant *oprD-pmcY* (DM3004) shows similar sensitivity to imipenem as the single mutant *oprD::dTn5*. Inhibition halos were photographed after 16 h incubation at 37°C. Similar sensitivities between mutant strains were obtained with increasing imipenem masses in the filter discs (not shown).

Figure 2. Conserved residues in the juxtamembrane region/domain (PmcYs) have a role in Zn^{2+} binding. (A) Left, conserved amino acids profile depicted in the structure for PmcY/PA3962. Positions colored with maroon indicates high conservation while cyan points to low conservation. Right, lateral chains of putative amino acids with metal binding capacity are shown. (B) Up, representation of the fusion protein GST-PmcYs. Down, metal (TM^{2+}) binding capacity and specificity of the fusion product. Metal bound to GST was subtracted in each case and represented 10% of the total metal present in GST-PmcYs. (C) Up, representation of the fusion protein with conserved amino acids positions indicated with blue lines. Down, binding capacity of mutants D40A, D47A and D65A. Notice that Zn^{2+} binding decrease to a half vs. WT. (D) Representation of putative Zn^{2+} binding sites in PmcY. Zn^{2+} atoms are indicated in red and putative bonds by O-ligands with dotted lines. In all cases, data are the mean ± SE of three independent experiments. **P*<0.01; $^{\#}$, *P*, 0.05 from a two-tailed Student's *t* test versus Zn^{2+} (B) or WT (C).

Figure 3. PmcY interacts with CzcS. On-column Zn^{2+}-dependent protein-protein interaction assay. (A) Upper and lower panel, 100 mg (200 µl) of resin bound with 10 nmole of GST-PmcYj ($PmcY_{30-93}$) were washed with 10 bed volume of Buffer B (Buffer A + 1 mM EDTA), (Upper panel, lane $REDTA_t$), or Buffer C (Buffer A + 0.1 mM Zn^{2+}) (Lower panel, lane $RZn^{2+}{}_t$) and incubated with 5 nmole $CzcS_{40-166}$ (lane +I). The flow through was collected (FT) and the resin washed 4X with 2 bed volumes of Buffer A (lanes W1-4). Finally, the resin was resuspended at the initial volume (lane Rf) and 25 µl of each fraction analyzed by SDS-PAGE 12% and CBB staining. Note that PmcY-CzcS interaction requires Zn^{2+} bound to PmcY (black asterisk). (B) Protein interaction analyses of PmcY mutants. EDTA treated (upper panel) or Zn^{2+}-loaded (lower panel) GST-PmcY mutants (5 nmole D40A, 1 nmole D47A, 2.5 nmole D65A) were incubated with 5 nmole CzcS. Twenty five µl of fractions from resin treated (lanes $REDTA_t$ and $RZn^{2+}{}_t$), incubated with CzcS (lanes +I) and final (lanes Rf) samples were analyzed as in (A). Black asterisk denotes the Zn^{2+}-dependent interaction and white, the lack of it.

Figure 4. PmcY-YiiP-like operons coevolved with OprD and likely CzcS in Pseudomonadales. Bioinformatic analyses. (A) Two operon configurations involving PmcY homologs were searched in complete bacterial genomes by multigene Blast using protein sequences; *pmcY-yiiP*-like operon (blue) and non-*pmcY-yiiP*-like operon (white). Parallel searches by RBH were done with protein sequences coded by *czcS* (green) and *oprD* (yellow). (B) Venn diagram showing the distribution of organisms with detected CzcS (green) and OprD (yellow) between the two configurations of PmcY (*pmcY-yiiP*-like operon, in blue vs. *non-pmcY-yiiP*-like

operon, in yellow). Note the lack of association between *non-pmcY-yiiP*-like operon organisms (226) with CzcS and OprD (1 and 13 organisms among 226, respectively). (C) Phylogenetic analysis of the organisms with PmcY homolog detected in the genome. Most species with *pmcY-yiiP*-like operon (blue strip) belongs to the order of Pseudomonadales (ocher). Coevolution of OprD and CzcS is depicted with yellow and green strips labels, respectively.

Figures

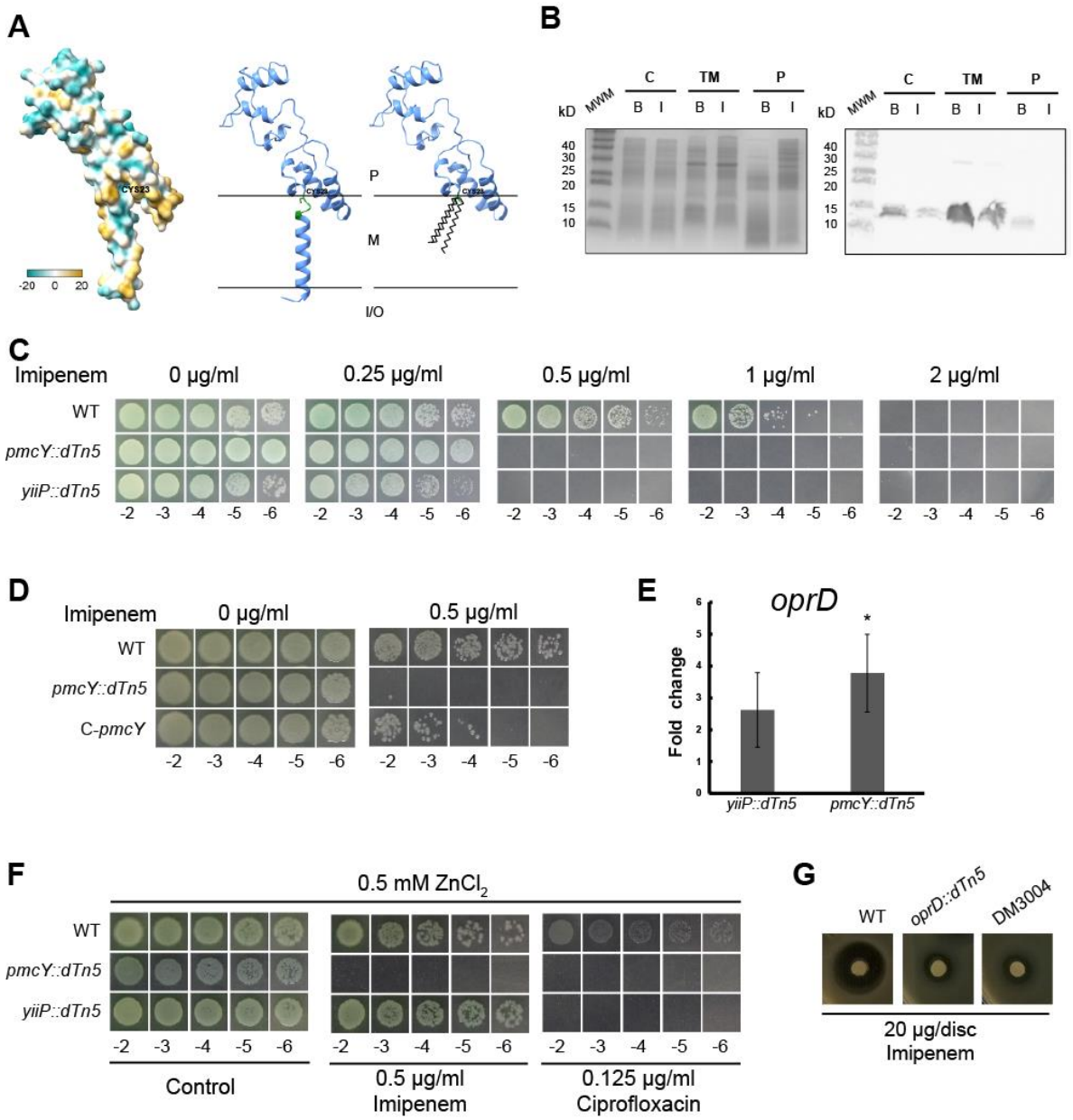

Figure 1

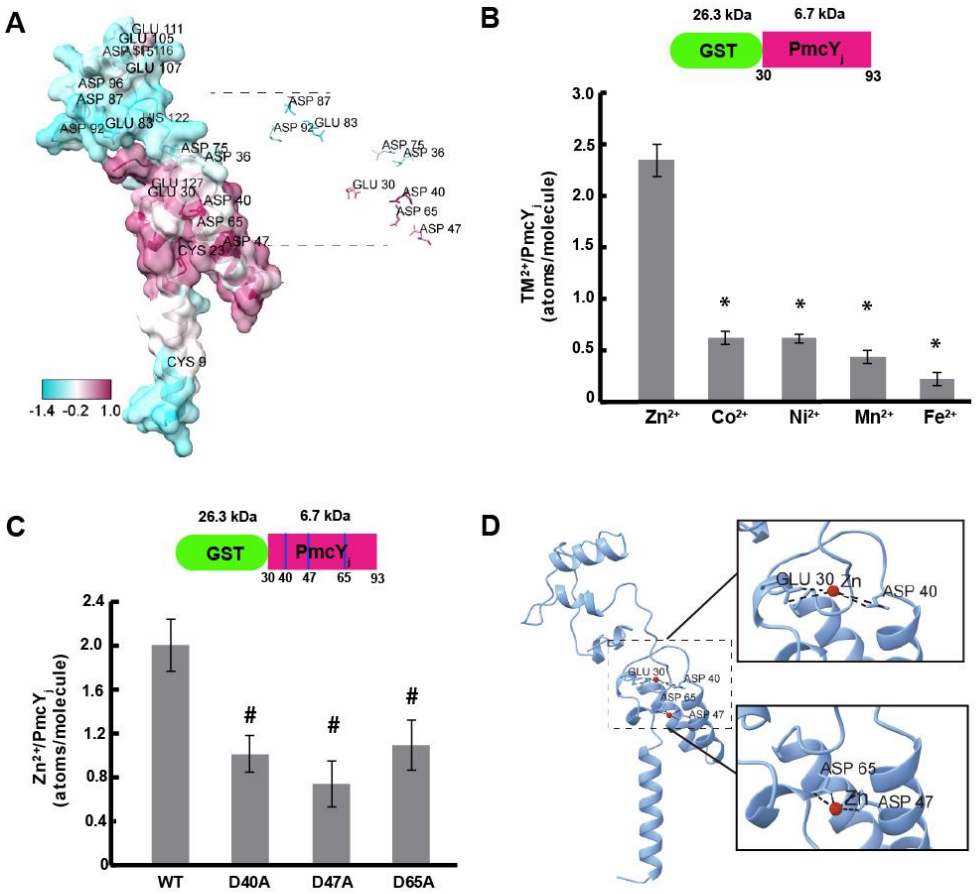
A
GLU 111
GLU 105
ASP 115
ASP 116
GLU 107
ASP 96
ASP 87
ASP 92
GLU 83
HIS 122
ASP 75
ASP 36
GLU 127
GLU 30
ASP 40
ASP 65
ASP 47
CYS 23
CYS 9
-1.4 -0.2 1.0
B
26.3 kDa
6.7 kDa
GST
PmcY
30
93
TM2+/PmcYj (atoms/molecule)
Zn2+
Co2+
Ni2+
Mn2+
Fe2+
C
26.3 kDa
6.7 kDa
GST
PmcY
30 40 47 65 93
Zn2+/PmcYj (atoms/molecule)
WT
D40A
D47A
D65A
D
GLU 30
Zn
ASP 40
ASP 65
ASP 47

Figure 2

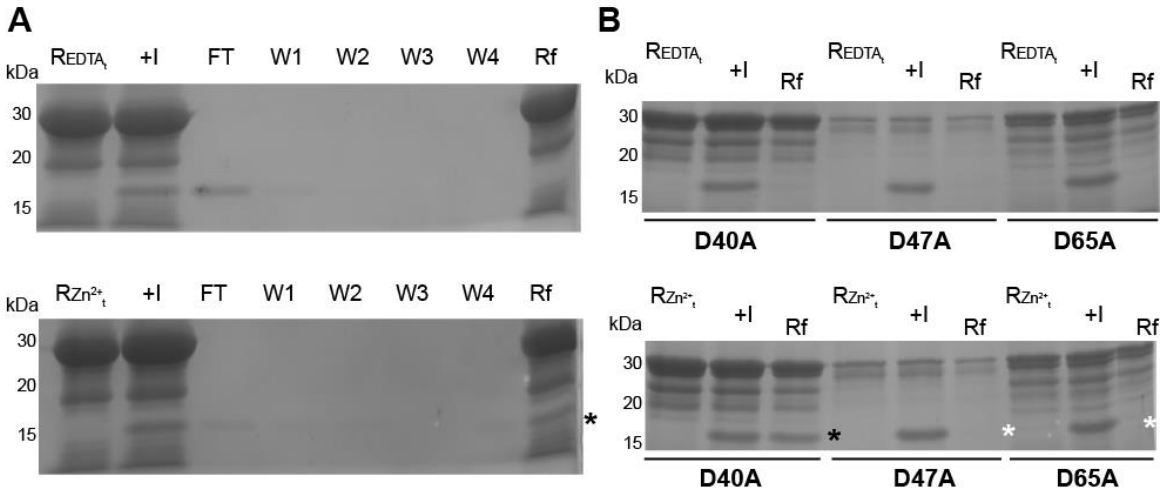

Figure 3

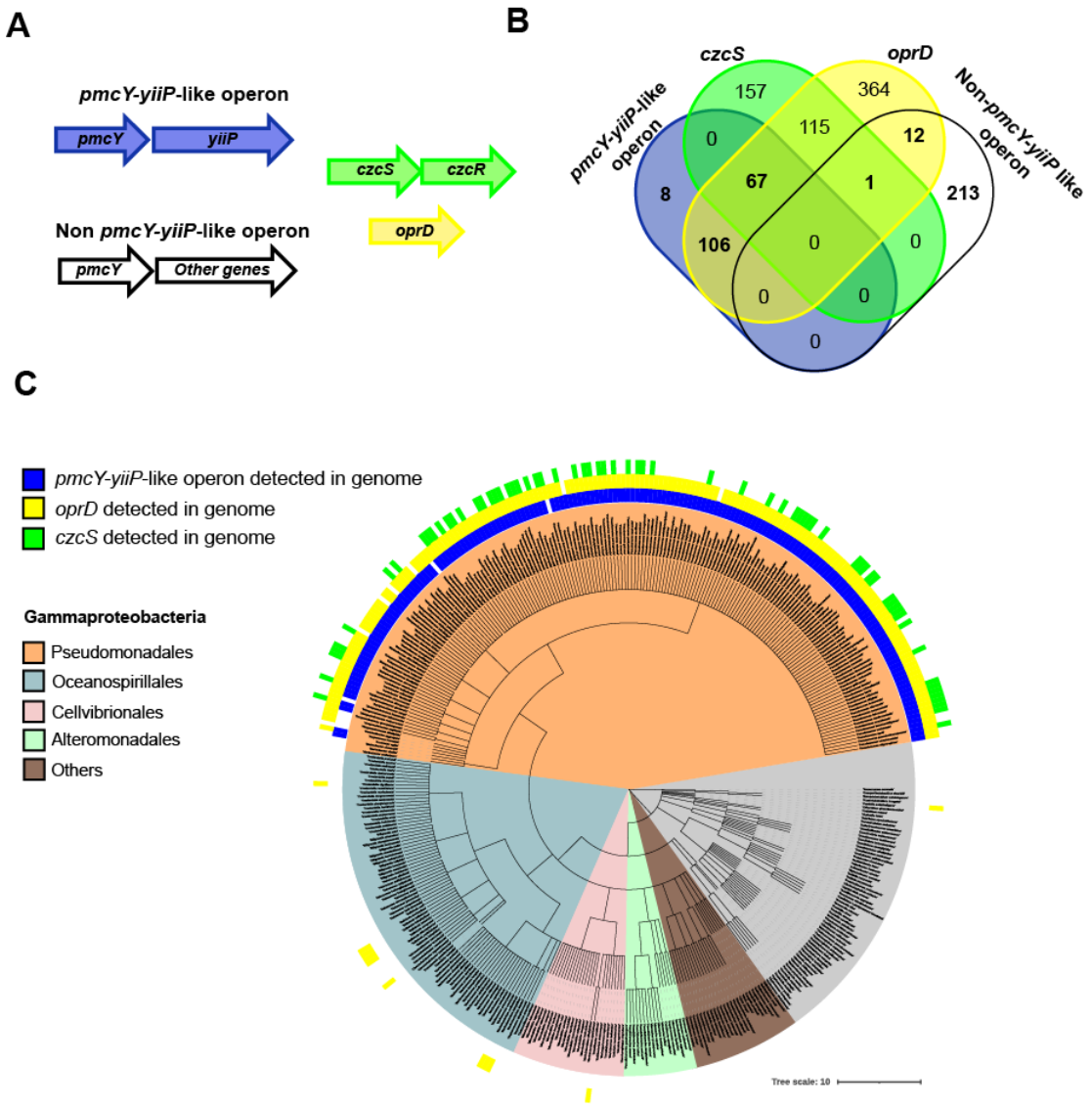
A
pmcY-yiiP-like operon
pmcY
yiiP
czcS
czcR
oprD
Non pmcY-yiiP-like operon
pmcY
Other genes
B
czcS
oprD
pmcY-yiiP-like operon
Non-pmcY-yiiP like operon
157
364
0
115
12
8
67
1
213
106
0
0
0
0
0
C
pmcY-yiiP-like operon detected in genome
oprD detected in genome
czcS detected in genome
Gammaproteobacteria
Pseudomonadales
Oceanospirillales
Cellvibrionales
Alteromonadales
Others
Tree scale: 10

Figure 4